The role of specific energy in micro-grinding of titanium alloy

Precision Engineering 72 (2021) 172–183

Contents lists available at ScienceDirect

Precision Engineering

journal homepage: www.elsevier.com/locate/precision

The role of specific energy in micro-grinding of titanium alloy

Mohammadali Kadivar [a,b,*], Bahman Azarhoushang [a], Uta Klement [b], Peter Krajnik [b]

[a] Institute of Precision Machining (KSF), Furtwangen University of Applied Sciences, Jakob-Kienzle-Str 17, 78056, Villingen-Schwenningen, Germany
[b] Department of Industrial and Materials Science, Chalmers University of Technology, Hörsalsvägen 7B, SE-412 96, Gothenburg, Sweden

ARTICLE INFO

Keywords:
Micro-grinding
Specific grinding energy
Dressing
Additive manufacturing
Titanium

ABSTRACT

This paper is concerned with understanding the role of specific energy in micro-grinding of conventional and additively manufactured Ti6Al4V. The effects of grinding and dressing parameters, cooling-lubrication conditions, and the directions of material build-up are studied. It is demonstrated that the minimum specific energy in single grain tests is independent of the material-fabrication method. The lowest measured specific energy obtained is 11.5 J/mm^3 for both workpiece materials. The direction of material build-up influenced the process only when grinding with low aggressiveness, where 20% higher specific energy was observed. Similar specific energies were obtained for oil-lubricated and dry conditions, indicating that lubrication had minimal effect. The effects of the diamond concentration in the wheel and the dressing parameters were also investigated. Comparable specific energies were observed for wheels with C150 and C200 concentrations. The specific energy was found being predominantly influenced by dressing. Coarse dressing conditions produced 18% lower specific energy and, therefore, a more efficient micro-grinding process.

1. Introduction

Ti6Al4V has distinctive properties such as high corrosion resistance, strength and ductility [1], making it a suitable choice for a wide range of applications such as biomedical, healthcare [2,3], microfluidic [4] and aerospace [5]. The machinability of titanium is associated with high specific energy, tool wear, poor surface finish, work-hardening, and burr formation [6]. However, machining of burr-free micro-features with a desireable surface finish is feasible by specially designed tools [7]. The machining of high-precision micro-parts from titanium alloys is especially challenging as it is accompanied by high plastic deformation due to the size effect [8,9], high tool deflection, and rapid tool wear [10]. Non-mechanical micro-manufacturing processes – such as lithography, Electro Discharge Machining (EDM) and Electro Chemical Machining (ECM) – are more expensive and time-consuming [11]. Therefore, the role of mechanical micro-machining processes is relevant and in focus here. Among various mechanical micro-machining processes, micro-grinding is considered a promising method for the production of high-quality parts where the geometrical (e.g. dimensional) and surface accuracies are demanding. Additional technology drivers are capabilities to cost-effectively manufacture complex 3D-geometries and micro-features. Obtaining tight tolerances through this method is also advantageous [12]. However, fundamental investigations into the application of micro-grinding are considered essential in order to further develop and understand the technology and meet industrial requirements.

The amount of available research in the field of micro-grinding is limited, despite recent interest in academia [13]. A novel laser-assisted micro-grinding process was developed by Kadivar et al. [14], which produced 60% lower grinding forces. The effect of crystallographic orientation on micro-grinding forces was studied by Zhao et al. [15]. They found out that the influence of the crystallographic orientation can be modeled precisely.

One of the most fundamental criterion for evaluating the machinability (or grindability) of micro-parts is the specific cutting (grinding) energy. The specific energy is defined as the energy expended to remove a unit volume of material, which is a fundamental parameter that indicates the efficiency of the material-removal process [16]. The required energy for material removal can be divided into three parts: rubbing, plowing and cutting [16]. An increase in the chip thickness reduces the relative proportions of friction and plowing energies and increases the proportion of cutting/chip-formation energy. A larger proportion of cutting energy leads to a higher process efficiency and is associated with an overall lower specific energy. In micro-grinding, a relatively high

* Corresponding author. Institute of Precision Machining (KSF), Furtwangen University of Applied Sciences, Jakob-Kienzle-Str 17, 78056, Villingen-Schwenningen, Germany.
E-mail address: kamo@hs-furtwangen.de (M. Kadivar).

https://doi.org/10.1016/j.precisioneng.2021.04.015
Received 10 December 2020; Received in revised form 15 April 2021; Accepted 20 April 2021
Available online 4 May 2021

specific energy is required for material removal compared to micro-machining (e.g. micro-milling) because of i) high elastic and plastic deformations in chip formation, and ii) high friction between the abrasive grains and workpiece because of the larger amount of rubbing and plowing. This phenomenon is common for all abrasive processes associated with a low chip thickness values [16,17]. Therefore, the specific grinding energy is considered as the main grindability parameter. Unfortunately, publications providing information on specific cutting energies for micro-grinding are almost nonexistent. This is in stark contrast to conventional grinding, where numerous publications report values for a variety of materials and grinding operations. The only known study that reports values of specific energy in micro-grinding was by Morgan et al. [18], for grinding tungsten carbide. The authors observed that the specific energy at the beginning of the wheel-workpiece contact was relatively high and then dropped rapidly to an almost constant value of 500 J/mm^3. This is much higher than the minimum energy of the macro-grinding process as described by Kadivar et al. [19] and Badger [20]. They reported minimum specific energies of 32 and 50 J/mm^3 for macro-grinding of tungsten carbide. Guo et al. [21] and Kacalak et al. [22] reported minimum values for titanium between 12 and 15 J/mm^3. Kadivar et al. [23] found a correlation between the surface integrity of the micro-ground parts and the specific cutting energy. They also concluded that using a lower cutting speed and higher feed rates leads to a better surface integrity at the same level of specific energy.

Another significant aspect of grindability of micro-parts is the material-manufacturing method. Additive manufacturing (AM) techniques offer a high degree of flexibility in manufacturing and provide the possibility to produce highly complex parts [24]. However, the AM-produced parts commonly yield a very high surface roughness. Moreover, in most cases AM parts are only at near-net shape and achieving tight tolerances is a challenge. Therefore, finishing operations are a necessary part of AM post-processing based on their capability to produce high-quality and precise functional surfaces. However, the machinability and grindability of AM-produced materials (at macro- and especially micro-scale) is still largely unknown. For example, Mallipeddi et al. showed a large influence on AM contour setting and thermal treatment on the machinability of Ti6Al4V [24,25]. Moreover, diverse AM processes (e.g. laser-based vs. electron-beam-based powder bed fusion) have specific effects on machinability in view of the process (e.g. power source, build direction) and the material's microstructure (grain size, micro-constituents). In view of focusing the state-of-the art review to machinability in micro-machining, it is fair to conclude that available research is very limited and restricted to the micro-milling process. Hojati et al. [26] studied the machinability of AM Ti6Al4V produced by the Electron Beam Melting (EBM) technique. They found no significant changes in the cutting forces for AM and conventional titanium at chip thicknesses ranging from 7.4 to 37.3 μm. However, better surface roughnesses were generated using EBM parts compared to the conventionally manufactured titanium. The machinability of Selective Laser Melting (SLM) parts compared to the cast Ti-alloy parts was examined by Le Coz et al. [27]. They showed that the cutting forces of SLM Ti6Al4V parts are higher than those of conventional parts, while the same chip morphology and almost the same surface quality were achieved for both materials. In contrast to other work, lower cutting forces were measured in micro-milling of Laser Engineering Net Shaping (LENS) titanium compared to conventional parts [28]. Thus, from the literature, it cannot be stated that the (micro-) machinability of the AM parts is necessarily different compared to conventional parts.

Based on the above, it is crucial to investigate the fundamental aspects of grindability (machinability) for materials produced by distinct manufacturing methods. This study is concerned with the investigation of the grindability of EBM and conventional (wrought) Ti6Al4V from the perspective of specific energy and surface quality. To gain a fundamental understanding of the chip-formation process, the micro-grinding tests are complemented with single-grain tests for both AM and conventional workpiece materials. The effects of cutting speed, the ratio of feed rate to depth of cut, dressing parameters, and grinding wheel concentration on grindability were investigated. The major indicator of grindability is the experimentally obtained curve of specific cutting energy vs. aggressiveness number. Moreover, to cover the widest possible application range, the experimental work further covered testing conditions over i) a wide span of grinding and dressing parameters, ii) two distinct grinding-wheel concentrations, and iii) different lubrication conditions (dry vs. straight-oil flood lubrication).

2. Materials investigated

Ti6Al4V grades produced by electron-beam melting (EBM) and conventional methods were chosen as the workpiece material. The conventional (wrought) material samples had the dimensions 30 × 20 × 10 mm. The AM samples had the dimensions of 30 × 20 × 4 mm in two different build directions: 1) build direction parallel to the workpiece length of 30 mm (AM BD 30); and 2) build direction parallel to the workpiece width of 20 mm (AM BD 20). The chemical composition of the material is listed in Table 1.

The samples were polished and etched for approximately 30 s using Kroll's reagent etchant (1–3 ml HF, 2–6 ml HNO_3, 100 ml DI water). The microstructure of the samples was investigated using an optical microscope. The microstructure of the AM material, shown in Fig. 1, reveals a thin acicular fine α-phase located perpendicular to each other (martensitic structure); however, the conventional part consisted of elongated alpha with intergranular beta, β. This highlights that the microstructure is highly dependent on the manufacturing method as a result of different cooling rates. After polishing and etching, the Vickers HV0.1 microhardness was measured The results were: for AM BD20, HV0.1 = 352±12; for AM BD 30 HV0.1 = 345±10. The conventional part has a microhardness of 340 HV±5. Based on these measurements, we can conclude that all material samples have almost the same Vickers hardness.

3. Experimental work

Two experimental setups were used for the micro-grinding and single-grain scratch tests. The micro-grinding tests utilized a KERN Pyramid Nano, high-precision, 5-axis, micro-machining center (Fig. 2a). Grinding and dressing parameters (Table 2) encompassed different cutting speeds (v_c), feed-rate-to-depth-of-cut ratios (v_w/a_e), dressing feed rates (v_{ftd}), and dressing speed ratios (q_d). The grinding tests employed the same aggressiveness. Prior to each test, the grinding wheel was dressed using a rotary dresser, i.e. a diamond form roller (Fig. 2b). The grinding wheel used was a vitrified diamond pin with a diameter of 2 mm, grain-size of 45 mm, at two different concentrations (C150 and C200). The grinding process was a peripheral, up-grinding operation with a width of 20 mm (Fig. 2c). Micro-grinding was performed using grinding oil as a lubricant.

The single-grain tests were performed on a Müga CNC milling machine (Fig. 2d). The experiments were carried out under dry and flood conditions (grinding oil). A fixed feed rate of 5000 mm/min was used to avoid overlapping of the scratches. A diamond grain with a pre-defined conical form with a tip diameter of 100 μm and a conical angle of 120° was used. The tool was mounted in a metal disk with a diameter of 150 mm. Prior to the tests, each material was polished to achieve a surface roughness of Ra ≈ 2 μm. Both micro-grinding and single-grain forces were measured using a Kistler dynamometer (type 9256C2).

After completing the single-scratch experiments with different depth

Table 1
Chemical composition (wt%).

Al	V	C	Fe	O	N	H	Ti
6	4	0.03	0.1	0.15	0.01	0.003	Balance

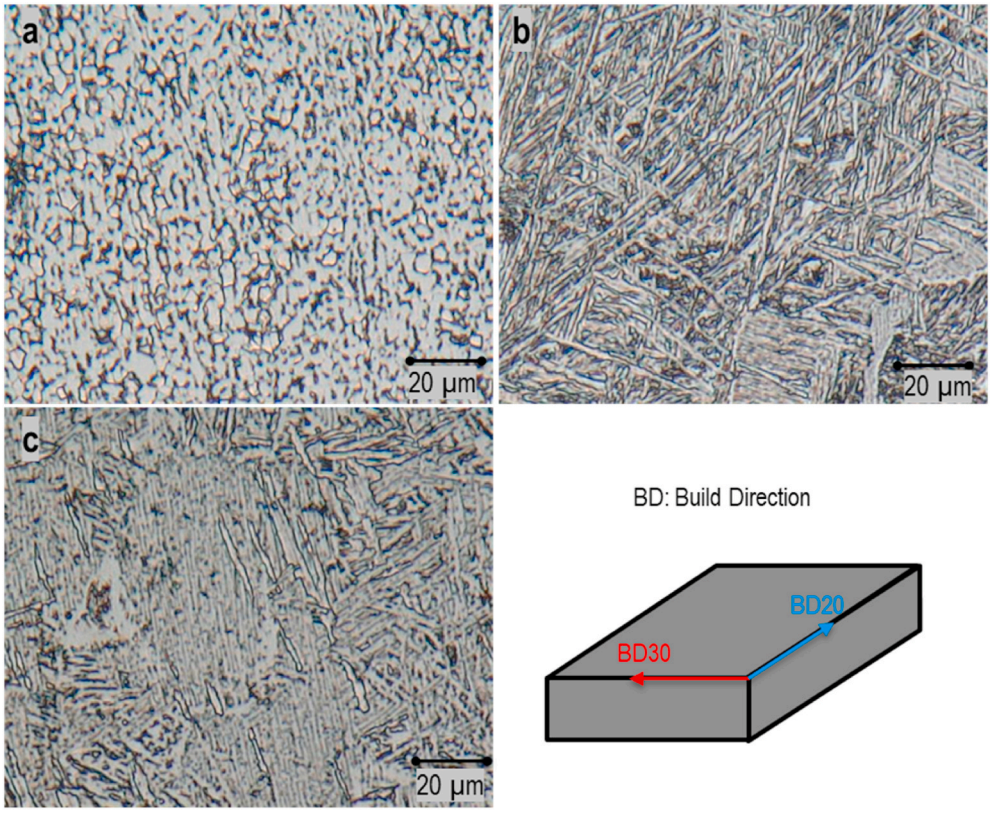

Fig. 1. The microstructure of a) conventional, b) AM BD 30, and c) AM BD 20 Ti6Al4V.

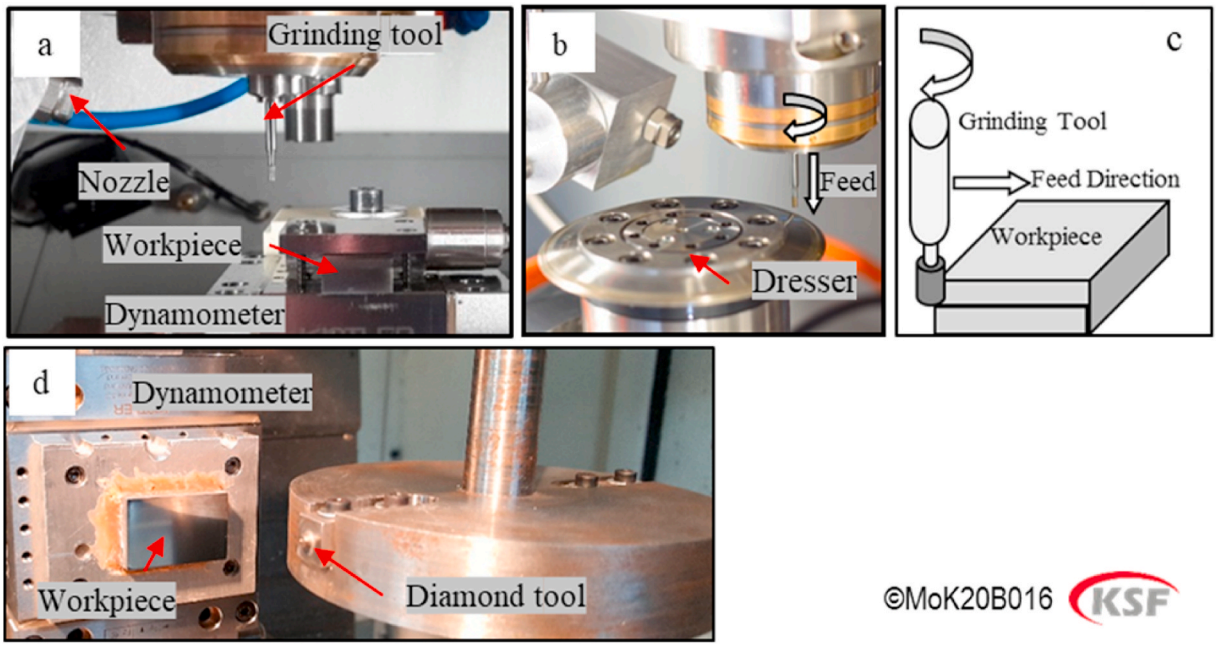

Fig. 2. a). Experimental setup of the micro-grinding process, b) dressing unit and kinematic, c) schematic of a peripheral micro-grinding, d) experimental setup for single grain tests.

of cuts, the scratches were measured using a confocal microscope (µsurf) with a 100 × 0.8 optical lens (i.e. 100× magnification at a distance of 0.8 mm). An exemplary scratch is illustrated in Fig. 3a. The polished surface of the workpiece sample was set as the zero plain and the image was divided into two sections. One section was used for measuring the pile-up volume (Fig. 3b) and the other section for measuring the volume of the removed material (Fig. 3c).

Table 2
Process parameters.

Parameters	Values
Micro-grinding wheel	D45-46-V-150 and - 200
Workpiece	Titanium grade 5 (Ti6Al4V)
Cutting speed (v_c) for micro-grinding	6, 10, and 14 m/s
Cutting speed (v_c) for single grain test	6 m/s
Feed rate to depth of cut ratio (v_w/a_e)	5, 8, and 11 (x10^4 mm/mm.min)
Axial depth of cut (a_p)	3.5 mm
Coolant for micro-grinding	Grinding oil
Coolant for single grain test	Dry, grinding oil
Dressing feed rate (v_{fd})	50 and 300 mm/min
Dressing speed ratio (q_d)	−0.4 and 0.8
Dressing depth of cut (a_{ed})	3 × 2 μm

4. Results and discussions

4.1. Single-grain scratching results

The single grain test was first carried out to experimentally determine the minimum specific energy required for cutting of titanium alloy and to fundamentally explain the results of a micro-grinding process. The evaluation of single-grain scratching and the explanation of the changes in specific cutting energy as an evaluation of the process efficiency requires the measurement the ratio of the volume of material removed to the volume of material piled-up. For this, the chipping ratio f_{ab} is used:

$$f_{ab} = \frac{V_s - V_p}{V_s} \tag{1}$$

where V_s and V_p are the volumes of the removed material (groove) and pile-up, respectively. The maximum value for the chipping ratio $f_{ab} = 1$ indicates no material pile-up in the absence of plastic deformation, i.e., ideal cutting. When $f_{ab} = 0$, no cutting occurs, and plastic deformation is the only mechanism leading to the piling-up of material. The efficiency of the chip formation process can be measured by the specific energy dissipated for scratching. Using the volume of removed material and tangential forces, the specific cutting energy for the single grain test can be calculated using the following equation:

$$u_c = \frac{v_c \cdot \int F_t dt}{V_s} \tag{2}$$

where v_c indicates the cutting speed and F_t is the tangential force. In single-grain scratching, the maximum depth of cut is equivalent to the chip thickness.

4.1.1. Material effects

Fig. 4 shows the results of the specific cutting energy and chipping ratio for the conventional and AM-produced titanium. As expected, the required specific energy for material removal was reduced by increasing the chip thickness for all materials. The minimum specific cutting energy of ~11.5 J/mm^3 was achieved for the titanium alloy regardless of the material-manufacturing method. The consumed energy for plastic deformation in the form of side plowing is larger than the energy required for the chip formation. As illustrated in Fig. 4b, the values of the chipping ratio vary with chip thickness. The chipping ratio increases with the chip thickness, leading to a more efficient chip formation and lower specific energy (as shown in Fig. 4a). The obtained chipping ratio for conventional parts is lower than those for the AM parts at chip thicknesses less than 5 μm. This is because of the different microstructures. Almost the same result for the chipping ratio was observed for both AM parts. As a result, the cutting of AM material is more efficient at lower chip thicknesses because of lower plastic and elastic deformation during the process. When cutting conventional material, the lower chipping ratio at low chip thicknesses resulted in a higher specific energy, where the share of plastic and elastic deformation is considerably larger compared to the share of cutting. For both additively-manufactured materials (AM BD 20 and AM BD 30), nearly the same specific energies were observed due to similar chipping ratio and hardness. In many cases, the AM-parts need to be fine finished. Examples of fine finishing of AM materials include super-finishing and fine grinding, which are performed at low chip thicknesses [17]. However, when larger chip thicknesses (larger than 5 μm) are used, the chipping ratio for the conventional part is slightly higher than for AM parts. This may be caused by the different material microstructures (Fig. 1). Interestingly, chip thicknesses higher than 5 μm resulted in higher chipping ratios for the conventional parts compared to the AM parts, where almost the same specific energies for all kind of materials were achieved. A higher chipping ratio generally means a more efficient process and lower specific energies. But at this point (chip thickness of 5 μm), the specific energy for all materials achieves its minimum value, which needs further investigation.

Malkin [14] and Shaw [16,29] pointed out that the minimum specific energy for the chip formation is associated with the melting specific energy of the material. The minimum specific cutting energy (11.5 J/mm^3) corresponds to the condition in which the friction and plastic deformation are minimal. The specific enthalpy of Ti6Al4V at different temperatures was already investigated by Boivineau et al. [30]. The specific melting energy of the workpiece material at a certain temperature can be determined by the difference of its specific enthalpy at room temperature. For the liquid-state, the specific melting energy of Ti6Al4V can be defined as:

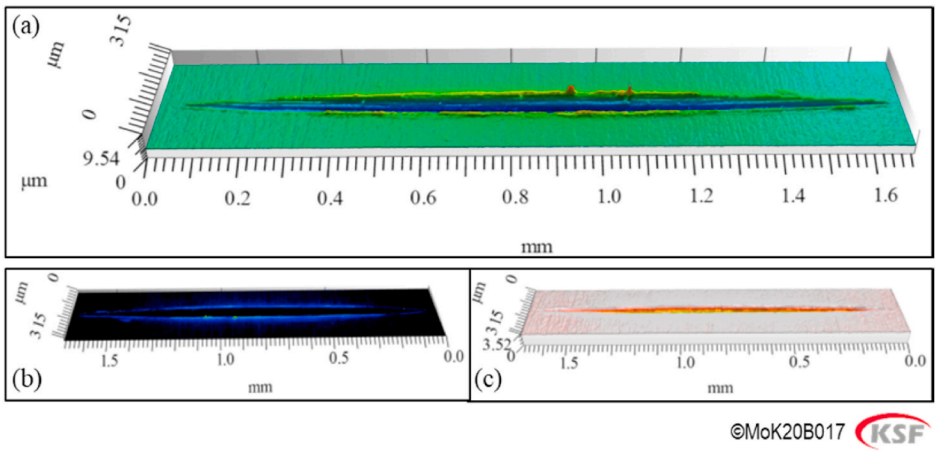

Fig. 3. a) Confocal image of the whole scratch, b) a section from zero plain to calculate the pile-up volume, and c) a section from zero plain to calculate the volume of removed material.

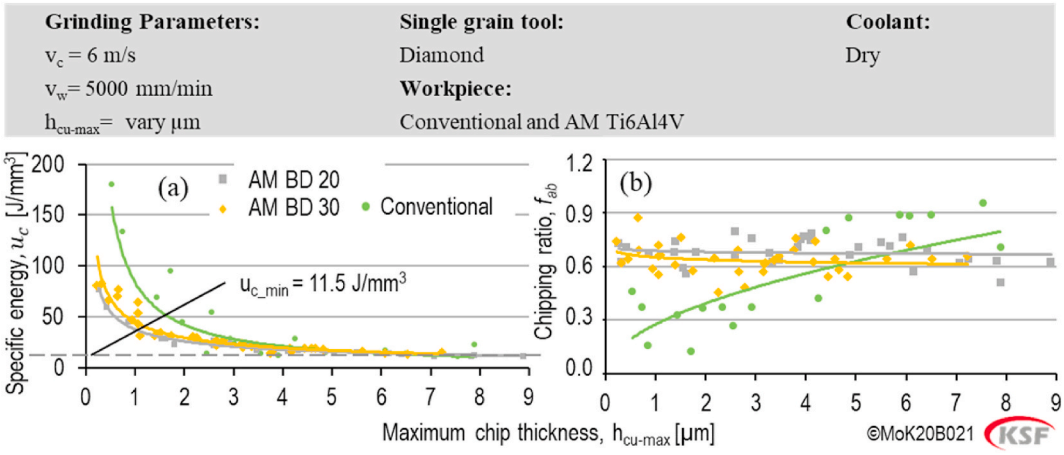

Fig. 4. The effect of the manufacturing process and chip thickness on a) the specific scratch energy and b) chipping ratio.

$$U_{liquidius} = H_{liquid} - H_{room} = 5.74\ J/mm^3 \quad (3)$$

The melting specific energy resembles the liquid state of Ti6Al4V for which the melting process is completed because the density of liquid titanium is much lower than in the solid-state. For the solid-state, the specific melting energy of the work material can be defined as:

$$U_{soli} = H_{soli} - H_{room} = 4.51\ J/mm^3 \quad (4)$$

where H_{room} is the enthalpy of Ti6Al4V at room temperature and H_{liquid} and H_{soli} are the enthalpies of Ti6Al4V at liquidus and solidus temperatures, respectively. $U_{liquidus}$ and U_{soli} denote the specific liquidus and solidus energies, respectively. Daneshi [31] modeled the time required for chip formation via each abrasive grain in grinding of nickel alloys. He pointed out that the time required for chip formation is much smaller than the time required for transformation from solidus to liquidus state. He mentioned that the minimum specific grinding energy can be limited to the specific solidus energy of each specific material. However, this minimum energy is approximately 35% higher than the specific solidus energy because of the friction between the abrasive grain and generated chip. The minimum specific cutting energy (11.5 J/mm^3) is much higher than the specific energy required for melting in both solidus and homologous states. Thus, this difference may be a result of high friction between the diamond cutting tool, the chips and the workpiece, as well as higher plowing or plastic deformation in the cutting process. Moreover, the tool has a defined geometry, i.e. a conical form with a relatively high negative angle (120°) and an ideal sphere tip radius of 100 µm without a sharp cutting. This would cause higher friction. However, in the actual grinding process, the individual cutting tools are much sharper.

4.1.2. *Cooling-lubrication effects*

The single-grain tests were carried out under dry and wet (oil as a lubricant) cooling-lubrication conditions. The results are illustrated in Fig. 5. Nearly the same chipping ratios were observed in all conditions. Moreover, the same specific energy was measured under dry scratching and when utilizing oil as a lubricant. Using oil as a lubricant decreases the friction between the tool and the workpiece and has a cooling effect during chip formation. However, it causes a higher plastic deformation. The single scratch tool, made of diamond, has a large negative rake angle. During cutting under dry conditions, the material experiences high friction between the tool and the workpiece in front of the tool – generating high temperatures. This high temperature may cause material softening. Additionally, because of the high friction between the tool and the workpiece, work hardening may occur. These combined effects lead to the same specific energy and almost the same chipping ratio as in the cutting process.

4.2. *Micro-grinding results*

Specific energy is a critical indicator of the grinding efficiency. Many factors – such as workpiece and grinding-wheel material, grinding and dressing parameters and wheel wear – influence the specific energy. The specific energy in grinding can be calculated as [16]:

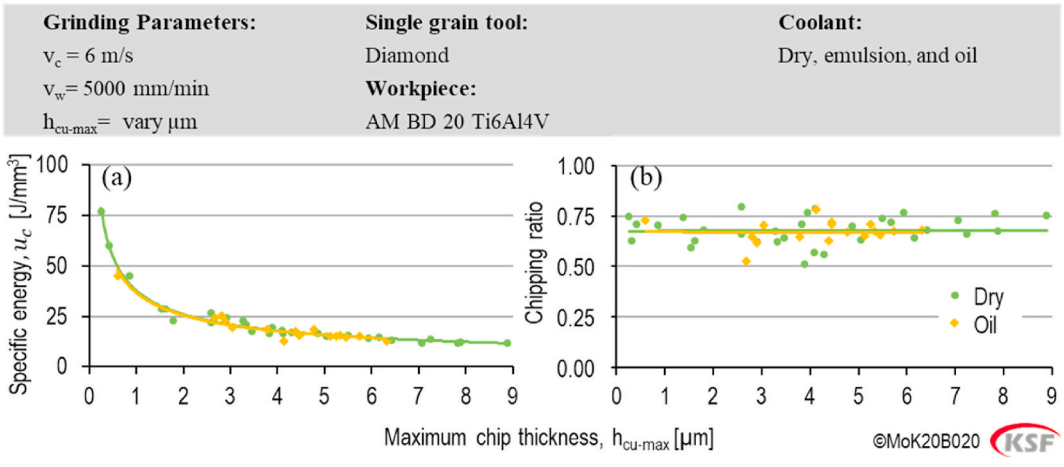

Fig. 5. The effect of lubrication method and chip thickness on a) the specific scratch energy and b) chipping ratio for the AM titanium BD 20.

$$e_c = \frac{F_t\, v_c}{Q_w} \tag{5}$$

where v_c is the wheel velocity, F_t is the tangential grinding force, and Q_w is the volumetric material removal rate.

The topography of the grinding wheel has random properties which make calculation of the chip thickness difficult. Therefore, the use of an alternative parameter to chip thickness can be useful to obtain a fundamental insight into the process from the perspective of geometry and kinematics. Drazumeric et al. [32] introduced a novel unifying modeling framework featuring the aggressiveness number, which can be directly related to the process outputs such the specific energy. In this study, the results of specific micro-grinding energy were compared under different conditions at the same grinding aggressiveness, calculated as [33]:

$$Aggr. = 1,000,000 \frac{v_w}{v_c} \sqrt{\frac{a_e}{d_s}} \tag{6}$$

where d_s is the effective diameter of the grinding wheel.

4.2.1. The effect of micro-grinding parameters

The ratio v_w/a_e is a valuable process-control parameter since the effect of both feed rate and depth of cut on the process outputs can be examined at the same time. The results of specific energy at different cutting speeds and feed-rate-to-depth-of-cut ratios were studied in our previous work [23]. According to the results, varying the cutting speed resulted in almost the same values of specific cutting energy with the same chip thicknesses (or same *Aggr*). The cutting-speed variation can change the share of friction and plastic deformation in the cutting process. This is due to different strain rates at different cutting speeds and/or the influence of the chip thickness, which can be observed using the specific energy values. According to the results presented in Ref. [23], changing the strain rate as a result of cutting speed does not change the flow stress of the Ti6Al4V. Thus, the cutting speeds used in this study can be counted as low and the flow stress follows the theory of the strain gradient plasticity. To have a better understanding of the process, the topography of the ground surface was assessed with help of the SEM images shown in Fig. 6. They show the effect of cutting speed at almost the same aggressiveness number, 21, and v_w/a_e ratio, 8×10^4mm/mm.min. To achieve almost the same aggressiveness at different cutting speeds, the feed rate and the depth of cut were increased in order to keep the v_w/a_e ratio constant. For example, at the cutting speed of 10 m/s, a v_w of 300 mm/min and an a_e of 3.8 μm resulted in and *Aggr*. of 21. To have almost the same *Aggr*. (19.5) at the cutting speed of 14 m/s, a v_w of 355 mm/min and an a_e of 4.4 μm were used.

A better surface quality with fewer surface defects was achieved at a cutting speed of 6 m/s (Fig. 6a). Increasing the cutting speed deteriorated the quality of the workpiece surface, where the chip thickness is almost the same [34]. Higher cutting speeds led to smeared material and cavities on the ground surface as a result of higher plastic deformation and possibly higher grinding temperature (Fig. 6b), despite almost the same grinding aggressiveness. More smeared material, larger cavities and some material debris can be seen when the cutting speed is 14 m/s (Fig. 6c) as compared to the cutting speeds of 6 m/s and 10 m/s (Fig. 6a and b). Therefore, at higher cutting speeds, high plastic deformation and higher temperatures are generated, resulting in material softening. However, it is important to note that the values of specific energy are identical for all cutting speeds. These results suggest that both material softening and strain hardening play a role in the cutting mechanism at the given cutting speeds.

Perhaps of more practical interest is the observation that the same specific energy was measured for all v_w/a_e ratios [23]. Increasing the v_w/a_e ratio increases the value of chip thickness slightly while the aggressiveness number is nearly constant [23,31,34]. However the changes are very small. For a better understanding of the effect of the v_w/a_e ratio, the topography of the finished surface was analyzed using SEM. The results are presented in Fig. 7. More smeared material was observed on the ground surface at lower v_w/a_e ratios, i.e. a lower surface quality is achieved during the cutting process when using a lower feed rate and a higher depth of cut. Hence, for increasing the material removal rate, it is recommended to use higher feed rates instead of higher depths of cut.

4.2.2. The effect of dressing parameters

In our previous work [35], the effect of dressing parameters on surface quality and grinding forces was investigated. Dressing parameters such as the dressing speed ratio, q_d, and the dressing overlap ratio, U_d, have a great influence on both surface quality and forces. However, the effects of dressing parameters on the specific energy and process efficiency are still largely unknown for micro grinding. The dressing

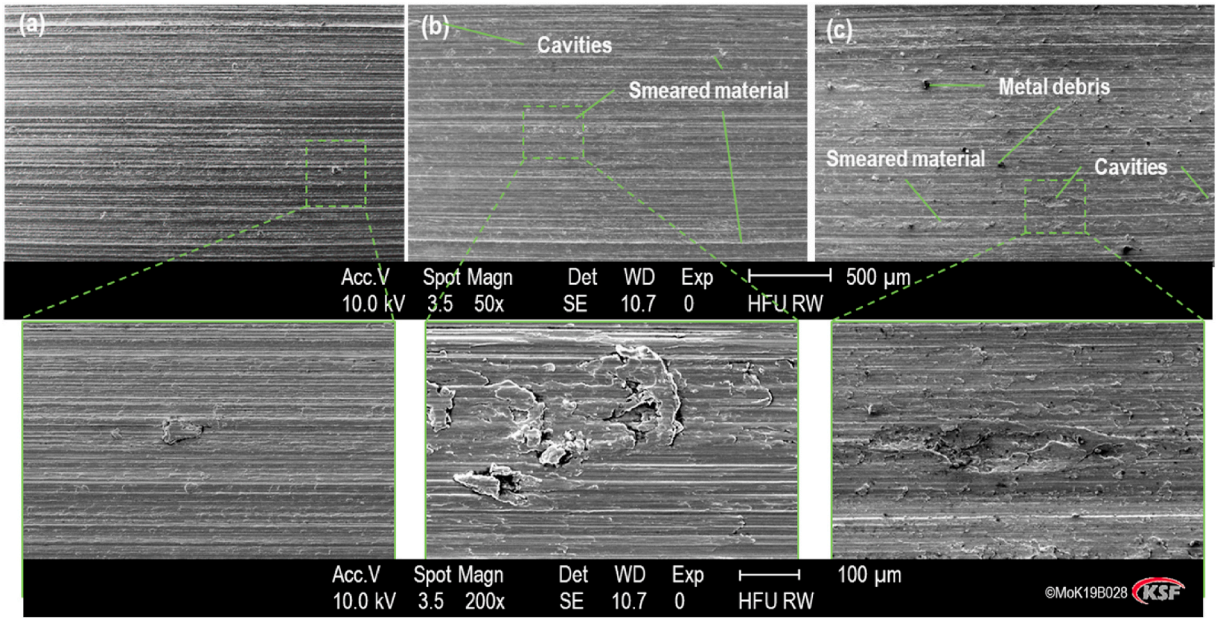

Fig. 6. Topography of the ground surface at (a) $v_c = 6$ m/s; (b) $v_c = 10$ m/s; (c) $v_c = 14$ m/s ($v_w/a_e = 8 \times 10^4$ mm/mm.min and *Aggr* ≈ 21).

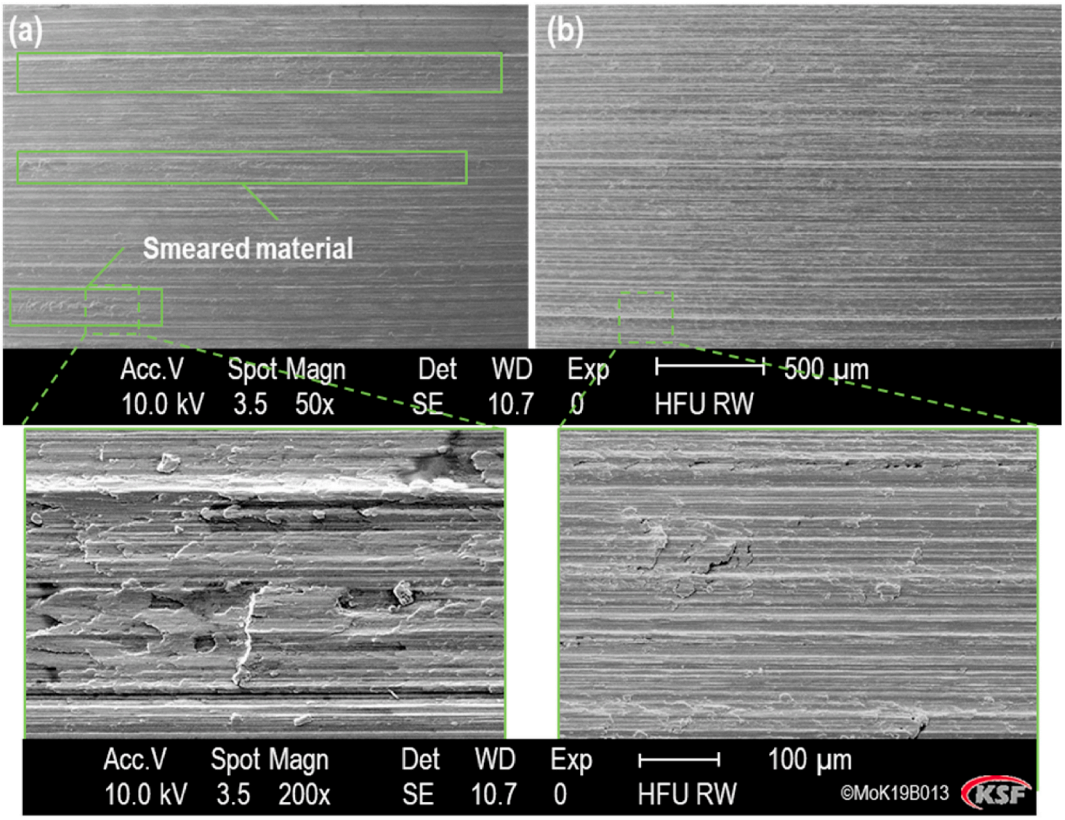

Fig. 7. SEM images of the ground surface at (a) $v_w/a_e = 5 \times 10^4$ mm/mm.min; (b) $v_w/a_e = 11 \times 10^4$mm/min.min ($v_c = 10$ m/s and *Aggr.* ≈ 21).

overlap ratio and speed ratio can be expressed as:

$$U_d \cdot = \cdot \frac{n_s \cdot \sqrt{(8 \cdot r_{pd} \cdot a_{ed})}}{v_{ftd}} \tag{7}$$

$$q_d \cdot = \cdot \frac{v_{cd}}{v_c} \tag{8}$$

where a_{ed} is the dressing depth of cut, r_{pd} is the radius of the dressing roll, v_{ftd} is the axial dressing feed rate, n_s is the rotational frequency of the micro-grinding wheel, and v_{cd} is the circumferential speed of the dressing roll.

The effect of the dressing method (up-dressing ($q_d < 0$) and down-dressing ($q_d > 0$)) as well as the dressing overlap ratios was investigated. In micro-dressing, achieving typical U_d values requires a very high rotational frequency of the grinding wheel since the diameter of the wheel is very small (i.e. 2 mm). Therefore, the dressing feed rate, v_{ftd}, is used in this study instead of U_d. The use of down-dressing and higher dressing feed rates resulted in lower specific energies. A rougher surface micro-topography and sharper cutting edges can be obtained by the down dressing method and a higher feed rate [35]. Rougher micro-topography and sharper cutting edges contribute to lower rubbing and elastic deformation in cutting, resulting in a more efficient process and, therefore, lower specific energies. Using the up-dressing method and higher overlap ratios (lower dressing feed rates) leads to a finer micro-topography of the micro-grinding wheel surface and, therefore, results in higher cutting forces [35]. A finer micro-topography increases the share of elastic and plastic deformation in the chip formation process and consequently causes higher specific energies, as shown in Fig. 8.

4.2.3. The effect of material microstructure

Fig. 9 shows specific-energy measurements for three different Ti6Al4V materials (conventional, AM BD 20, and AM BD 30) for two different wheel concentrations (150C in Figs. 9a and 200C in Fig. 9b).

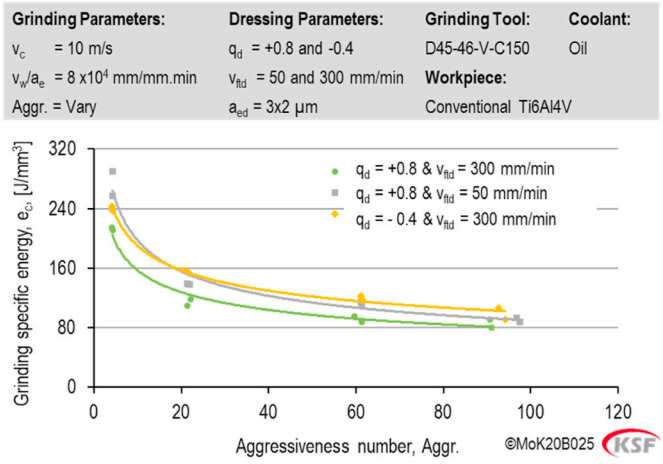

Fig. 8. The effect of dressing parameters on the micro-grinding specific energy.

Increasing the grinding aggressiveness resulted in lower specific energies, which were also observed in the single-grain scratch tests by increasing the chip thickness (Fig. 4). Higher aggressiveness values cause less rubbing and less plastic deformation in chip formation – and consequently a more efficient grinding process. With an increase in the aggressiveness number, a minimum specific grinding energy of 79 J/mm^3 was achieved, which is much higher than the minimum specific energy in the single-grain scratch tests (11.5 J/mm^3). This is because of the size effect in the micro-grinding process. Achieving the minimum specific grinding energy is only possible at aggressive process conditions that minimize plowing and rubbing. In the micro-grinding process, which features a small wheel diameter and high tool deflection, obtaining high aggressiveness values is not feasible due to limitations in

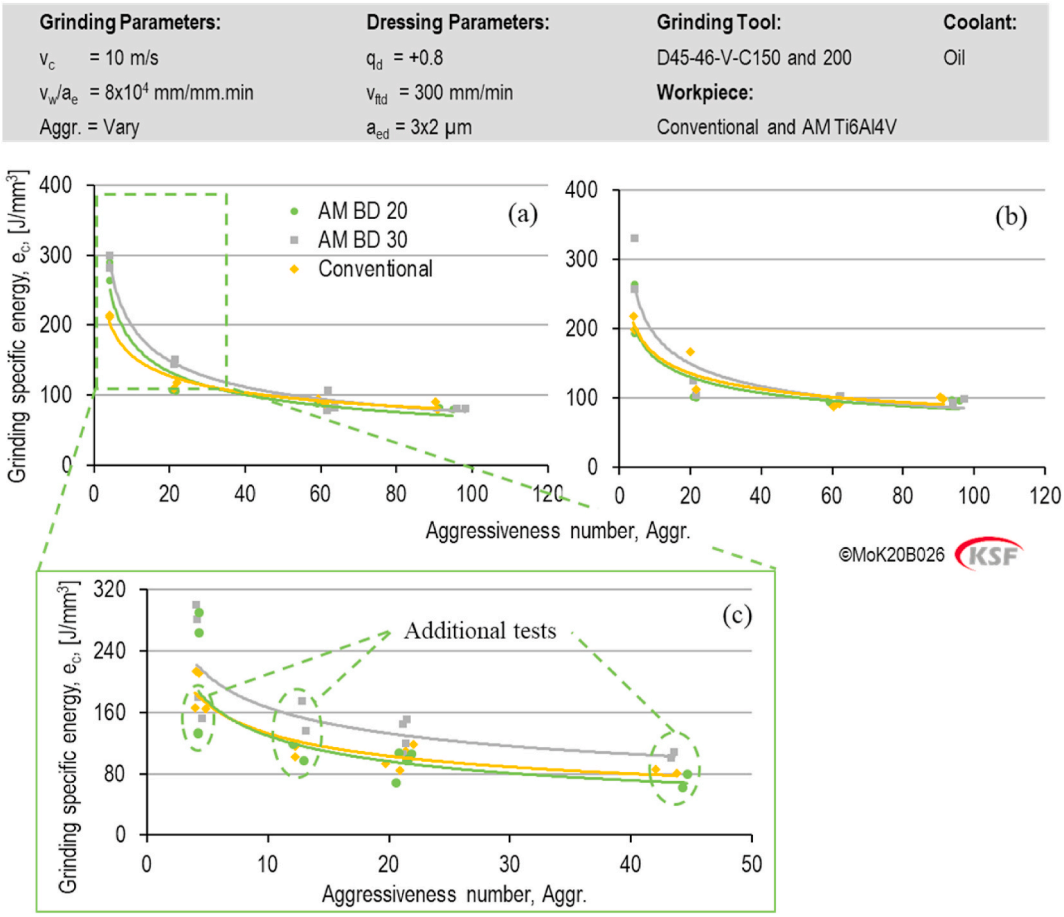

Fig. 9. The effect of the manufacturing process on the specific energy: a) for the 150-concentration wheel, b) for the 200-concentration wheel, and c) the 150-concentration wheel in detail.

the achievable depth of cuts and feed rates.

In contrast to the single-grain scratch tests, where the AM materials generated lower specific energies compared to conventional titanium, the specific cutting energy in AM parts was either equal (for titanium build parallel to the workpiece width of 20 mm) or higher (for titanium build parallel to the workpiece length of 30 mm, and only for small aggressiveness numbers) in micro-grinding. At higher aggressiveness values, almost the same values of specific micro-grinding energy were obtained for all samples. The same can be observed for the 200-concentration wheel (Fig. 9b). To check the validity of the results for non-aggressive grinding conditions (i.e. low aggressiveness), additional tests were done. The results are presented in Fig. 9c. The results confirm that at low aggressiveness values, the highest specific energy in the micro-grinding process was generated in the case of AM BD 30.

The differences between the specific energies in the single grain scratch test and in micro-grinding can be explained by the chipping ratio in the single-grain scratch test. Contrary to micro-milling, the chip thickness in the micro-grinding process is normally very low (typically lower than 2 µm) [23]. Therefore, to examine the material-removal mechanism, small chip thicknesses in the single grain scratch test must be considered. According to the results in Fig. 4, at chip thicknesses lower than 5 µm the AM parts produced lower pile-up material compared to the conventional part – independent of the build direction. In this range, the specific energies of AM parts are also lower because of the lower share of plastic deformation in the single-grain scratch tests. In the single-grain scratch tests, only a single abrasive grain participates in the cutting process in a single cutting path. In the micro-grinding process, however, the grinding wheel consists of several abrasive grains (for example 20 static abrasive grains in 10 µm depth of the tool) which are stochastically distributed over the surface of the grinding wheel. Hence, several abrasive grains are contributing to the cutting process simultaneously.

As with the single-grain scratch test, a slot remains after each grain-workpiece engagement. The 3D space includes a groove and material pile-up left along the cutting path (Fig. 10b). The subsequent abrasive grain then engages with the work material. The new grain, depending on its protrusion height and position with respect to the first grain, either cuts another slot along its moving path or moves between the slots cut by the former grains. If the grain comes into contact with the workpiece, it will not only cut the workpiece surface but also remove the pile-up material remaining from the previous pass (visualized in red in Fig. 10c). The higher the volume of piled-up material, the higher will be the volume of material removed by successive grains. This results in a larger instantaneous chip thickness for each abrasive grain under the same cutting conditions.

Varying the chip thickness changes the share of the rubbing, plowing and cutting in chip formation. Since the chipping ratios for the conventional part are smaller than the chipping ratios for the AM parts (at chip thicknesses values lower than 5 µm, in Fig. 4b), each single abrasive grain removes relatively more material (i.e., there is more pile-up material at the same chip thicknesses), which means a higher share of cutting and a lower share of plastic and elastic deformation. The micro-grinding of conventional parts benefits in this respect. However, it could result in a higher share of plastic deformation in the micro-grinding of AM parts. Therefore, the specific micro-grinding energies are almost of the same order as the conventional parts. Another reason may be associated with strain hardening. Dmitriev et al. [36] studied the effect of material crystallographic orientation on strain hardening of pure

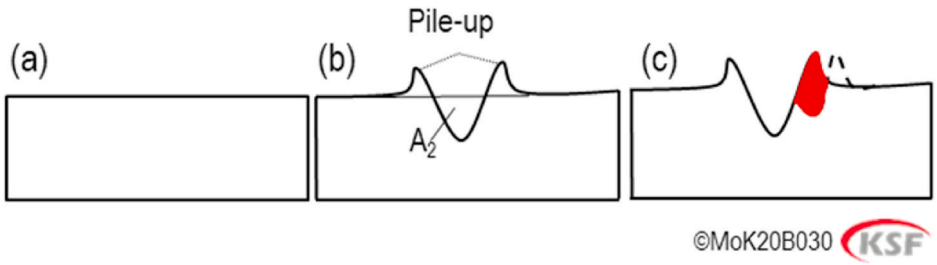

Fig. 10. Schematic of cutting path section a) material/blank prior to the grinding, b) after the first cut, and c) removed material by the following grain.

titanium in scratch tests. They showed that, depending on the crystallographic orientation, the strain hardening after scratching can happen either on the base material or the pile-up. It was also reported that when the indenter (here in micro-grinding the abrasive grains) moves along the easy-slide directions (the easy-to-cut crystallographic orientations), the strain hardening happens in the base material rather than in the pile-up. Moreover, when the indenter movement differs from easy glide directions, then the strain hardening happens in the pile-up materials.

Fig. 11 shows the microstructure of the grove section after single-grain scratch tests for different materials. Since the AM-produced materials have an acicular microstructure, while the conventional materials consist of elongated alpha with intergranular beta, the orientation of the grains in piled-up material for the AM parts could be different than in a conventional part. These orientations may reveal the strain hardening on the pile-up material of AM parts. The pile-up material, which is much harder than the base material in the case of AM because of the strain hardening, will be removed via successive grains in the micro-grinding process, resulting in higher specific energies. However, a larger affected depth (more compressed grains) can be observed on the base material under the grove in the case of the conventional material, resulting in material hardening in the finished surface.

The topography of the ground surface for the three materials was analyzed and the results are displayed in Fig. 12. Almost the same surface topography was achieved using the same grinding parameters, regardless of the material-manufacturing method. The surface parameter, Sa, and roughness parameters, Ra and Rz, are all nearly of the same order. In all cases, some material debris can also be seen on the ground surface.

The effect of wheel concentration (amount of abrasive contained in the wheel) on the specific micro-grinding energies is shown in Fig. 13. Interestingly, changing the wheel concentration resulted in almost the same specific energies for the cutting speeds of 10 and 14 m/s.

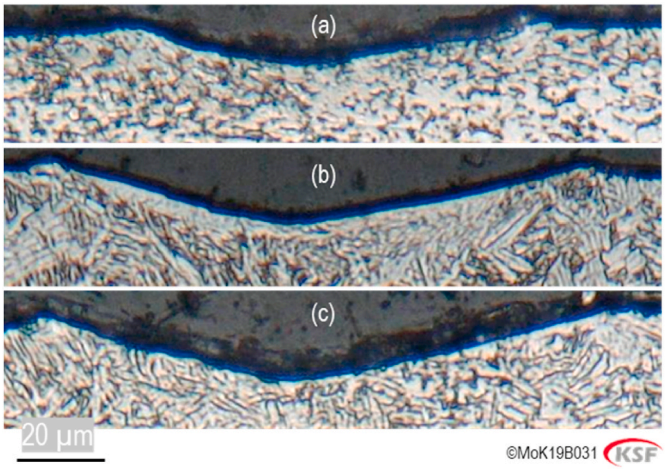

Fig. 11. Microstructure of the grove section by the single grain scratch test for a) conventional Ti6Al4V, b) AM BD 30 Ti6Al4V, and c) AM BD 20 Ti6Al4V (v_c = 6 m/s).

According to the discussion above, the specific energy is highly dependent on the chip thickness and topography of the micro-grinding wheel (Fig. 8). Therefore, to find an explanation for the same specific energies observed, the maximum chip thickness has to be analyzed.

It is worth to mention that the aggressiveness number does not capture the effect of wheel micro-topography on cutting forces, specific cutting energy and surface roughness. Hence, to compare the grinding results where the grinding wheel specification and dressing parameters are not the same, the chip thickness is a more appropriate parameter. The chip thickness changes with varying the grinding parameters (i.e. the feed rate, v_w, cutting speed, v_c, depth of cut, a_e, equivalent diameter of the grinding wheel, d_s) and wheel topography (i.e. cutting-point density, C, and the chip-shape factor, r) as described in equation (9). Since the geometry and kinematics of the process are the same (i.e. same aggressiveness number), the chip thickness is changing with the micro-topography of the grinding wheel.

$$h_m = \left[\frac{6}{C \cdot r}\left(\frac{v_w}{v_c}\right)\left(\frac{a_e}{d_s}\right)^{1/2}\right]^{1/2} \tag{9}$$

The higher the concentration, the higher the number of dynamic grains participating in the chip formation, resulting in higher C and lower chip thickness. Since the wheel was dressed with the same dressing parameters, we assume similar shape of the grains, hence the r factor should be approximately identical for both micro-grinding wheels. Decreasing the chip thickness causes a larger share of elastic and plastic deformation in the grinding process. Hence, increasing the wheel concentration at the same aggressiveness number should theoretically increase the values of specific energy. Both micro-grinding wheels were analyzed using a confocal microscope after micro-grinding within *Aggr.* of nearly 50 (see Fig. 14). For the 200-concentration wheel, a number of the abrasive grains were pulled-out after just one grinding pass. The pulled-out grains caused a reduction in the static and, consequently, dynamic grain density. Hence, the values of specific energy are of the same order.

This can be also observed in Fig. 15 where similar surface roughnesses were observed for both grinding wheels. A larger number of dynamic grains normally improves the quality of the finished surface. The reason is related to the lower chip thickness from the higher concentration. It can also be concluded that the number of active grains is almost equal for both wheels since the values of the surface roughness are approximately identical for both wheels. The higher grain pull-out in the wheel with higher concentration may be attributed to accumulated grains in a certain area of the grinding wheel. A higher number of grains causes lower cutting force acting on each abrasive grain. However, it also increases the risk of chip loading since the wheel has lower porosity. The loaded chip and accumulated grains may lead to stress concentration on a specific area and eventually grain pull-outs.

5. Conclusions

The grindability of conventional and AM-produced Ti6Al4V in micro-grinding was investigated, with the following conclusions:

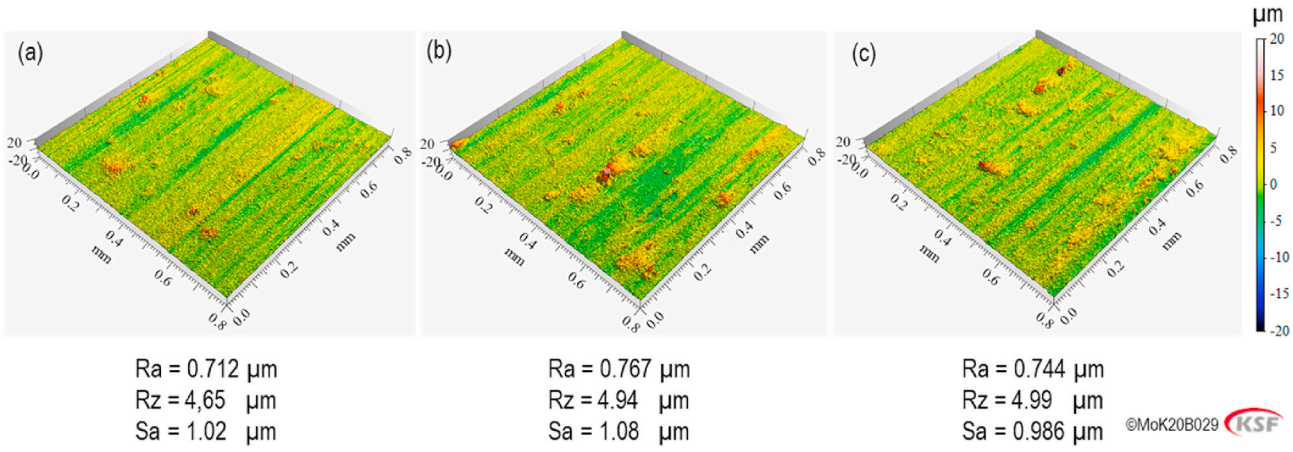

Fig. 12. Surface topography of the workpiece after micro-grinding process for a) conventional part, b) AM BD 20, and c) AM BD 30 ($v_c = 10$ m/s, $a_e = 10$ µm, $v_w = 800$ mm/min, and *Aggr.* ≈ 100).

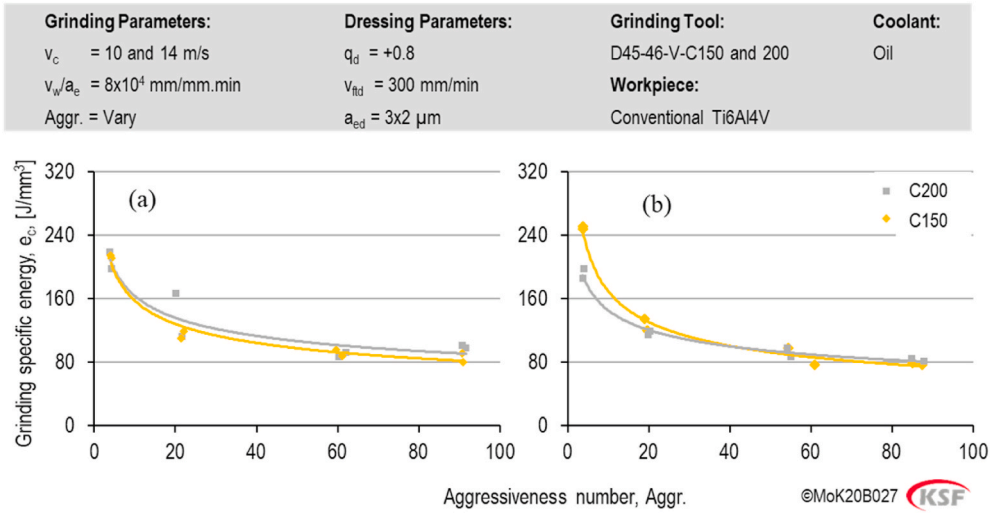

Fig. 13. The effect of wheel concentration on the specific energy a) $v_c = 10$ m/s, and b) $v_c = 14$ m/s.

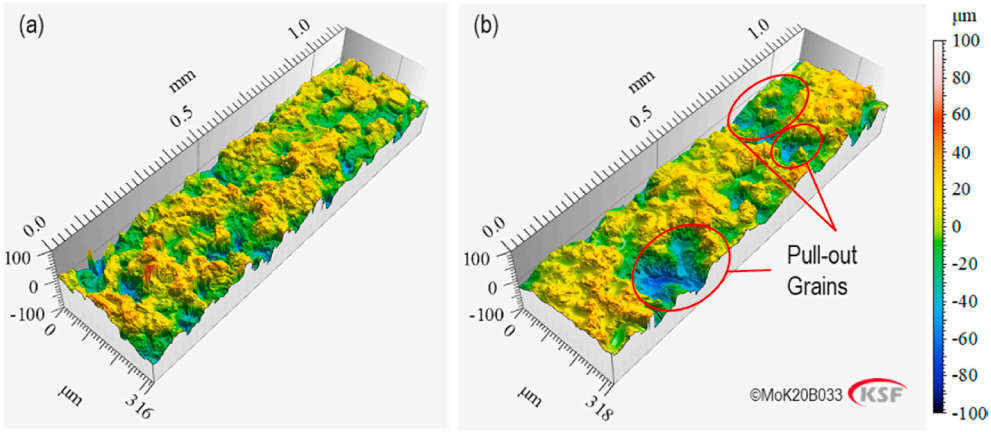

Fig. 14. The micro-topography of the wheel with a) concentration of 150 and b) concentration of 200 after grinding process with $v_c = 10$ m/s, $a_e = 6$ µm, $v_w = 480$ mm/min, and Aggr. ≈ 44.

- The same minimum specific energy of 11.5 J/mm^3 was obtained in the single-grain scratch for both workpiece materials (conventional and AM-produced) owing to their same hardness. Cutting of AM material was more efficient (by approximately 40%) compared to conventional material at chip thicknesses lower than 5 µm. This was due to approximately 50% higher chipping ratios and lower specific energies.

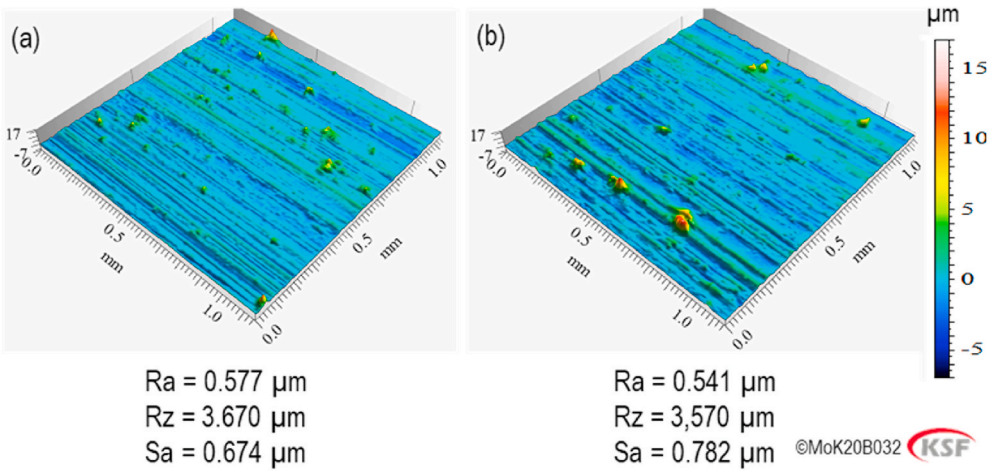

Fig. 15. Surface topography of the workpiece after the micro-grinding process for a) the wheel with a concentration of 150, b) the wheel with a concentration of 200 (conventional Ti6Al4V, $v_c = 10$ m/s, $a_e = 6$ μm, $v_w = 480$ mm/min, and Aggr. ≈ 44).

- In micro-grinding, the build direction of the AM parts had a significant influence on the specific energy at low aggressiveness (20% higher specific energy in case of AM BD30 compared to conventionally-produced part), which is contrary to the observations in the single-grain test where the AM parts generated 40% lower specific energies. However, at higher aggressiveness values, almost the same specific energy was obtained for all materials.
- Higher cutting speeds resulted in larger plastic deformation, causing more smeared material and cavities as well as metal debris on the ground surface. High-quality surfaces (without defects) were only achieved at a low cutting speed of 6 m/s.
- Grinding with a sharp wheel (achieved by up-dressing using high dressing feed rates) gave 18% lower specific energies. The wheel concentration did not affect the obtained specific energies.
- To increase the material removal rate, it is recommended to use higher feed rates rather than larger depths of cut. Using larger depths of cut results in a worse surface quality, even with a similar specific energy.

Declaration of competing interest

The authors declare that they have no known competing financial interests or personal relationships that could have appeared to influence the work reported in this paper.

Acknowledgment

The authors would like to thank Arcam AB for supplying the additive-manufactured titanium and Meister Abrasives AG for providing the grinding wheels. The authors would like to express their sincere gratitude to Mr. Alexander Filbert from Furtwangen University for his help in the metallographic investigations.

References

[1] Kadivar M. Micro-grinding of titanium. Chalmers University of Technology; 2018.
[2] Niinomi M. Recent research and development in titanium alloys for biomedical applications and healthcare goods. Sci Technol Adv Mater 2016;4(5):445–54. https://doi.org/10.1016/j.stam.2003.09.002.
[3] Rack HJ, Qazi JI. Titanium alloys for biomedical applications. Mater Sci Eng C 2006;26(8):1269–77. https://doi.org/10.1016/j.msec.2005.08.032.
[4] Zhang YT, Bottausci F, Rao MP, Parker ER, Mezic I, Macdonald NC. Titanium-based dielectrophoresis devices for microfluidic applications. Biomed Microdevices 2008;10(4):509–17. https://doi.org/10.1007/s10544-007-9159-y.
[5] Voice W. The future use of gamma titanium aluminides by Rolls-Royce. Aircraft Eng Aero Technol 1999;71(4):337–40. https://doi.org/10.1108/00022669910371031.
[6] Ezugwu EO, Wang ZM. Titanium alloys and their machinability—a review. J Mater Process Technol 1997;68(3):262–74. https://doi.org/10.1016/S0924-0136(96)00030-1.
[7] Aziz M, Ohnishi O, Onikura H. Innovative micro hole machining with minimum burr formation by the use of newly developed micro compound tool. J Manuf Process 2012;14(3):224–32. https://doi.org/10.1016/j.jmapro.2011.12.006.
[8] Zhang T, Liu Z, Shi Z, Xu C. Investigation on size effect of specific cutting energy in mechanical micro-cutting. Int J Adv Manuf Technol 2017;91(5–8):2621–33. https://doi.org/10.1007/s00170-016-9934-0.
[9] Zhang T, Liu Z, Xu C. Influence of size effect on burr formation in micro cutting. Int J Adv Manuf Technol 2013;68(9–12):1911–7. https://doi.org/10.1007/s00170-013-4801-8.
[10] XI X, Ding W, Wu Z, Anggel L. Performance evaluation of creep feed grinding of γ-TiAl intermetallics with electroplated diamond wheels. Chin J Aeronaut 2020. https://doi.org/10.1016/j.cja.2020.04.031.
[11] Masuzawa T. State of the art of micromachining. CIRP Ann. 2000;49(2):473–88. https://doi.org/10.1016/S0007-8506(07)63451-9.
[12] Hoyle R. Developments in micro and nano engineering and manufacturing. Plast., Rubber Compos. 2013;37(2–4):50–6. https://doi.org/10.1179/174328908X283302.
[13] Pratap A, Patra K, Dyakonov AA. A comprehensive review of micro-grinding: emphasis on toolings, performance analysis, modeling techniques, and future research directions. Int J Adv Manuf Technol 2019;104(1–4):63–102. https://doi.org/10.1007/s00170-019-03831-x.
[14] Kadivar M, Shamray S, Soltani B, Daneshi A, Azarhoushang B. Laser-assisted micro-grinding of Si3N4. Precis Eng 2019;60:394–404. https://doi.org/10.1016/j.precisioneng.2019.09.004.
[15] Zhao M, Ji X, Liang SY. Influence of AA7075 crystallographic orientation on micro-grinding force. Proc IME B J Eng Manufact 2018;233(8):1831–43. https://doi.org/10.1177/0954405418803706.
[16] Malkin S, Guo C. Grinding technology: theory and application of machining with abrasives. Industrial Press Inc; 2008.
[17] Hashimoto F, Yamaguchi H, Krajnik P, Wegener K, Chaudhari R, Hoffmeister H-W, et al. Abrasive fine-finishing technology. CIRP Ann. 2016;65(2):597–620. https://doi.org/10.1016/j.cirp.2016.06.003.
[18] Morgan CJ, Vallance RR, Marsh ER. Specific grinding energy while microgrinding tungsten carbide with polycrystalline diamond micro tools. In: ICOMM-2007 2nd International Conference on micro-manufacturing; 2007. p. 180–7.
[19] Kadivar M, Azarhoushang B, Daneshi A. Study of specific energy in grinding of tungsten carbide. In: 14th International Conference on high speed machining, 17-18th April 2018. Kursaal, san Sebastian - Spain.
[20] Badger J. Grinding of sub-micron-grade carbide: contact and wear mechanisms, loading, conditioning, scrubbing and resin-bond degradation. CIRP Ann. 2015;64(1):341–4. https://doi.org/10.1016/j.cirp.2015.04.007.
[21] Guo GQ, Liu ZQ, Zheng XH, Chen M. Investigation on surface grinding of Ti-6Al-4V using minimum quantity lubrication. AMR (Adv Magn Reson) 2012;500:308–13. https://doi.org/10.4028/www.scientific.net/AMR.500.308.
[22] Kacalak W, Lipiński D, Bałasz B, Rypina Ł, Tandecka K, Szafraniec F. Performance evaluation of the grinding wheel with aggregates of grains in grinding of Ti-6Al-4V titanium alloy. Int J Adv Manuf Technol 2018;94(1–4):301–14. https://doi.org/10.1007/s00170-017-0905-x.
[23] Kadivar M, Azarhoushang B, Daneshi A, Krajnik P. Surface integrity in micro-grinding of Ti6Al4V considering the specific micro-grinding energy. Procedia CIRP 2020;87:181–5. https://doi.org/10.1016/j.procir.2020.02.069.
[24] Horn TJ, Harrysson OLA. Overview of current additive manufacturing technologies and selected applications. Sci Prog 2012;95(Pt 3):255–82. https://doi.org/10.3184/003685012X13420984463047.
[25] Mallipeddi D, Hajali T, Rännar L-E, Bergström A, Hernandez S, Strandh E, et al. Surface integrity of machined electron beam melted Ti6Al4V alloy manufactured

with different contour settings and heat treatment. Procedia CIRP 2020;87:327–32. https://doi.org/10.1016/j.procir.2020.02.091.
[26] Hojati F, Daneshi A, Soltani B, Azarhoushang B, Biermann D. Study on machinability of additively manufactured and conventional titanium alloys in micro-milling process. Precis Eng 2020;62:1–9. https://doi.org/10.1016/j.precisioneng.2019.11.002.
[27] Le Coz G, Fischer M, Piquard R, D'Acunto A, Laheurte P, Dudzinski D. Micro cutting of Ti-6Al-4V parts produced by SLM process. Procedia CIRP 2017;58:228–32. https://doi.org/10.1016/j.procir.2017.03.326.
[28] Bonaiti G, Parenti P, Annoni M, Kapoor S. Micro-milling machinability of DED additive titanium Ti-6Al-4V. Procedia Manuf. 2017;10:497–509. https://doi.org/10.1016/j.promfg.2017.07.104.
[29] Shaw MC. Principles of abrasive processing. Oxford: Clarendon Press; 1996.
[30] Boivineau M, Cagran C, Doytier D, Eyraud V, Nadal M-H, Wilthan B, et al. Thermophysical properties of solid and liquid Ti-6Al-4V (TA6V) alloy. Int J Thermophys 2006;27(2):507–29. https://doi.org/10.1007/PL00021868.
[31] Daneshi A. Micro chip formation mechanism in grinding of Nickel-base superalloy-Inconel 718. Albert-Ludwigs-Universität Freiburg; 2019.
[32] Dražumerič R, Badger J, Roininen R, Krajnik P. On geometry and kinematics of abrasive processes: the theory of aggressiveness. Int J Mach Tool Manufact 2020;154:103567. https://doi.org/10.1016/j.ijmachtools.2020.103567.
[33] Badger J. Practical application of aggressiveness and chip thickness in grinding. In: J. Badger. CIRP 3rd International Conference high performance cutting (HPC), Dublin, Ireland; 2008. p. 599–606.
[34] Kadivar M, Azarhoushang B, Krajnik P. Modeling of micro-grinding forces considering dressing parameters and tool deflection. Precis Eng 2020;67:269–81. https://doi.org/10.1016/j.precisioneng.2020.10.004.
[35] Kadivar M, Azarhoushang B, Shamray S, Krajnik P. The effect of dressing parameters on micro-grinding of titanium alloy. Precis Eng 2018;51:176–85. https://doi.org/10.1016/j.precisioneng.2017.08.008.
[36] Dmitriev AI, Nikonov AY, Shugurov AR, Panin AV. Numerical study of atomic scale deformation mechanisms of Ti grains with different crystallographic orientation subjected to scratch testing. Appl Surf Sci 2019;471:318–27. https://doi.org/10.1016/j.apsusc.2018.12.021.